Hindawi Publishing Corporation
Mathematical Problems in Engineering
Volume 2016, Article ID 5284815, 13 pages
http://dx.doi.org/10.1155/2016/5284815

Research Article

Impact of Different Static Air-Gap Eccentricity Forms on Rotor UMP of Turbogenerator

Yu-Ling He, Wei-Qi Deng, Gui-Ji Tang, Xiao-Ling Sheng, and Shu-Ting Wan

Department of Mechanical Engineering, North China Electric Power University, Baoding 071003, China

Correspondence should be addressed to Yu-Ling He; heyuling1@163.com

Received 11 May 2016; Accepted 16 June 2016

Academic Editor: Zhike Peng

Theoretical analysis and numerical FEM calculations, together with segmental experiment studies, are used to study the impact of the static air-gap eccentricity forms on the rotor unbalanced magnetic pull (UMP) of turbogenerator. The universal expression of the magnetic flux density under different forms of SAGE is firstly deduced, based on which the detailed UMP formulas for the normal condition and three SAGE cases are obtained, respectively. Then the exciting characteristics of the UMP for each SAGE form to generate vibrations are analyzed. Finally, numerical FEM calculations and segmental experiments are carried out to investigate the effect of SAGE forms on the rotor UMP, taking the SDF-9 type non-salient-pole fault simulating generator as the object. It is shown that, no matter what kind of SAGE occurs, amplitude increments at each even harmonic component of the UMP and the rotor vibration, especially the 2nd harmonic component, will be brought in. Meanwhile, the UMP keeps directing to the very position where the minimum radial air-gap is. Among the different SAGE forms, the rotor offset has the most sensitive effect on the rotor UMP and vibration, while the stator ellipse deformation has the weakest impact.

1. Introduction

Due to the assembly quality, the bearing damage, and the performing environments, most generators are running under an air-gap eccentricity condition [1]. The air-gap eccentricity, which is also usually named as rotor eccentricity by many scholars, appears as the air-gap is larger on one side but meanwhile smaller on the other side. For example, the bearing offset or the stator core deformation can cause a typical static air-gap eccentricity [2]. A very tiny air-gap eccentricity will not bring in serious impact on the generator's regular performing. However, when the eccentricity degree is more than 10% of the total air-gap length, severe vibrations, stator core deformations, and even winding damage will be caused [3]. Therefore, accurate monitoring and timely control on this kind of fault is of significance.

In most cases, the air-gap eccentricity is usually mentioned in the radial direction and can be divided into three types, that is, the static air-gap eccentricity (SAGE), the dynamic air-gap eccentricity (DAGE), and the mixed air-gap eccentricity (MAGE) [4, 5]. In this paper, we mainly focus on the static one.

By far, achievements of the monitoring and diagnosis on the air-gap eccentricity fault primarily focus on the stator current [6] and voltage [7, 8], the rotor current [8] and the shaft voltage [9], the inductance variation of the windings [10, 11], and the rotor UMP and vibration analysis [12–14]. The inductance variation is mainly based on the winding function theory [15] and the improved winding function theory [16, 17] and needs a large amount of calculation, while the current and the voltage analysis is actually based on the harmonic changes of the magnetic flux density [6]. The direct analysis on the spectrum of the stator and rotor current or voltage obtained via Fourier transform can sometimes hardly exactly identify the eccentricity due to the inconspicuous amplitude change comparing with the noise signal magnitude, especially when the capacity of the generator is not so large or the eccentricity is not so severe. To overcome this disadvantage, scholars developed an improved method based on the search coil [18]. However, this method needs to install extra components, that is, the search coil, in the generator, which requires a higher cost and is not welcomed by the practical performers in the power plant because it has to stop the generator for the specific installation work. Comparatively, the method

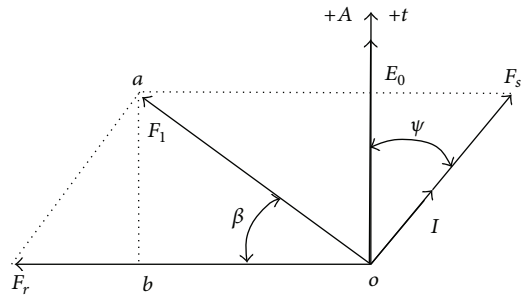

Figure 1: MMFs in normal condition.

based on the rotor vibration is more convenient because most generators have already installed vibration sensors before the generator is put into operation. Even if extra vibration sensors are needed to be installed in addition, there is no need to stop the generator but just to fix the sensors at the bearing block. Therefore, many researchers have paid much attention to the rotor UMP [19, 20] which is the essential cause of the rotor vibration and the rotor dynamics with UMP [21, 22].

However, people have only considered the eccentricity condition caused by the rotor side such as the rotor offset or asymmetry, while other potential causes are mostly ignored. That is why air-gap eccentricity is usually also named as rotor eccentricity by many scholars. Taking SAGE as an example, scholars primarily focus on the rotor offset form [23, 24], while the stator deformation conditions are not taken into account. Actually, since the stator has radial vibrations at $2f$ (f is the electrical frequency) even in normal condition [25], the hollow stator core which is composed of lots of fan-shape silicon steel sheets and fixed by double-screw bolts and frames will probably have a concave deformation or a convex deformation after a long suffering from the continuous vibration and the magnetic pull [26]. Specifically, due to the slot harmonic effect on the magnetic pull [27] and the elliptical rotating magnetomotive force caused by the asymmetric 3-phase currents [28], the stator will be dragged into an ellipse form after a long period performance [27, 28]. Then another problem appears. What is the effect of different eccentricity forms on the rotor UMP? Which kind of air-gap eccentricity has the most sensible impact on the rotor UMP?

The intent of this paper is to investigate the impact of SAGE forms, including rotor offset, stator concave deformation, stator convex deformation, stator ellipse deformation, and mixed SAGE composed of rotor offset and stator deformation, on the rotor UMP characteristics. Also, the sensitivity of these SAGE forms acting on the UMP is studied.

2. Theoretical Analysis

2.1. Magnetic Flux Density (MFD) Analysis. According to [2], the air-gap magnetomotive force (MMF) in normal condition indicated in Figure 1 can be expressed as

$$\begin{aligned} f(\alpha_m, t) &= F_r \cos(\omega_r t - \alpha_m) \\ &\quad + F_s \cos\left(\omega_r t - \alpha_m - \psi - \frac{\pi}{2}\right) \\ &= F_1 \cos(\omega_r t - \alpha_m - \beta) \\ F_1 &= \sqrt{F_s^2 \cos^2\psi + (F_r - F_s \sin\psi)^2} \\ \beta &= \operatorname{arctg}\frac{F_s \cos\psi}{F_r - F_s \sin\psi}, \end{aligned} \tag{1}$$

where F_r, F_s, and F_1 are, respectively, the rotor MMF, the stator MMF, and the composite MMF at the fundamental frequency, $\omega_r = 2\pi f_r$ is the rotor mechanical angular frequency, f_r is the rotating frequency of rotor (for turbogenerator, f_r equals the electrical frequency f, and hereafter, we write f_r as f and ω_r as ω for short), α_m is the mechanical angle to indicate the circumferential location of the air-gap, and ψ is the internal power angle of the generator.

Theoretically, in addition to the fundamental frequency component, the MMF still has other odd harmonics such as the 3rd, 5th, and 7th, with the amplitudes gradually decreased. Since the values of the higher harmonics are much smaller than the fundamental harmonic, we ignore these higher harmonics for convenience.

In this paper, we consider different forms of SAGE, respectively, caused by rotor offset, stator deformation, and the mixed condition of these two, as indicated in Figure 2. Specifically, the stator core ellipse condition, which includes the concave deformation and the convex deformation at the same time and frequently appears in generators, is actually a special case of stator core deformation. There are four SAGEs (see Figure 2(e)). For the sake of universality, considering the possible SAGE cases together, the radial air-gap length can be written as

$$g(\alpha_m) = g_0 \left[1 - \delta_s \cos\alpha_m - \sum \delta'_{sn} \cos(\alpha_m + \theta_n)\right], \tag{2}$$

where g_0 is the average value of the air-gap, δ_s is the relatively static eccentricity caused by rotor offset, δ'_{sn} is the relatively static eccentricity caused by stator deformation (δ'_{sn} denotes reducing the air-gap, while $-\delta'_{sn}$ denotes increasing the air-gap), n is the total number of the stator static eccentricities, and θ_n is the angle between the nth stator static eccentricity and the x-axis.

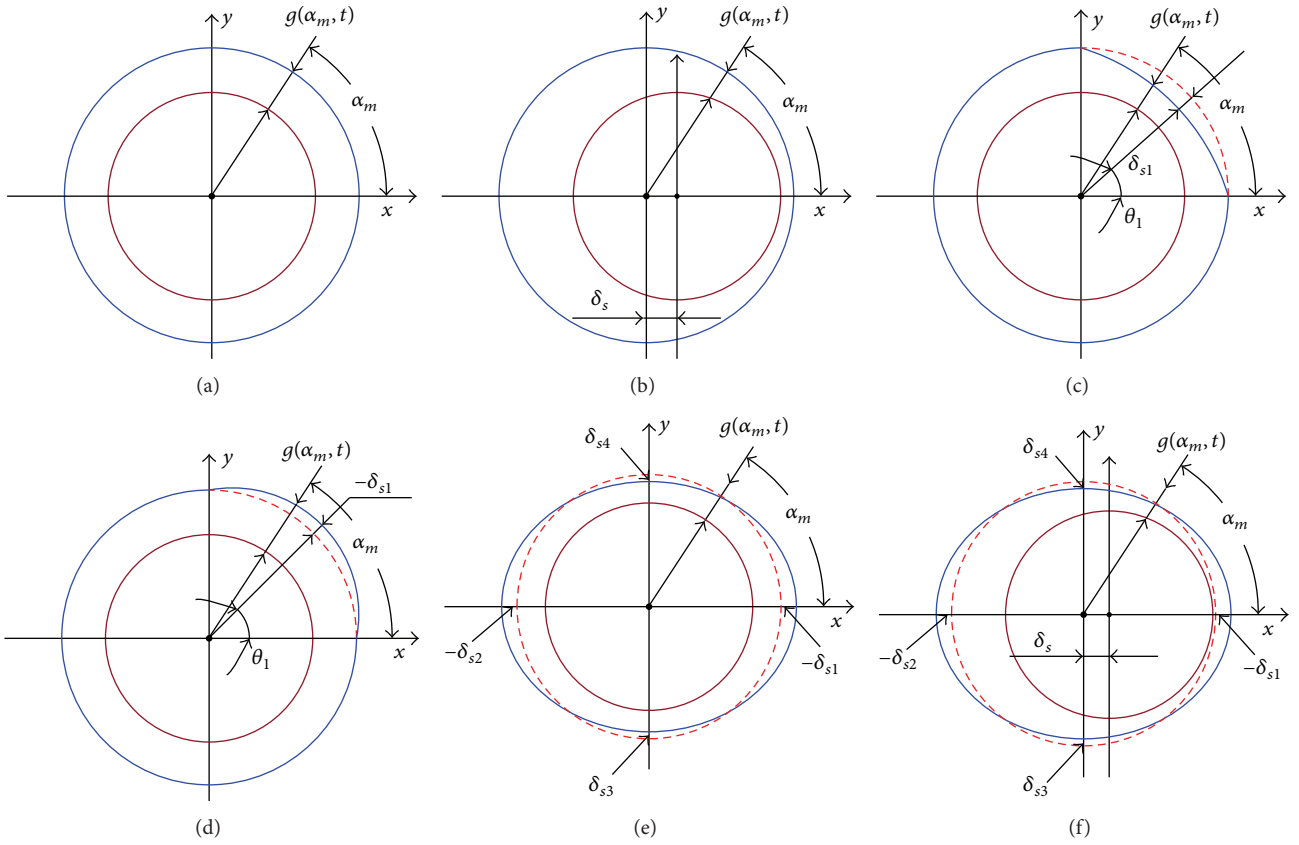

FIGURE 2: Different forms of SAGE in generator: (a) normal, (b) SAGE caused by rotor offset, (c) SAGE caused by stator core concave, (d) SAGE caused by stator core convex, (e) SAGE caused by stator core ellipse, and (f) mixed SAGE example caused by rotor offset and stator core ellipse.

The air-gap permeance can be obtained by means of power series expansion, and ignoring the higher order components it can be finally written as

$$\Lambda(\alpha_m) = \frac{1}{g(\alpha_m)} = \Lambda_0 + \Lambda_s \cos\alpha_m + \sum \Lambda'_{sn} \cos(\alpha_m + \theta_n), \tag{3}$$

where Λ_0 is the constant component of the air-gap permeance, $\Lambda_s = \Lambda_0 \delta_s$ is the component of the permeance caused by rotor offset, and $\Lambda'_{sn} = \Lambda_0 \delta'_{sn}$ is the component caused by stator deformation.

Objectively, (3) is an approximate formula because the higher harmonics such as $\Lambda_s \cos^2\alpha_m$ and $[\sum \Lambda'_{sn} \cos(\alpha_m + \theta_n)]^2$ have been ignored. Usually, the air-gap eccentricity is relatively small (large air-gap eccentricity, e.g., more than 30%, will most potentially cause the protective equipment of the generator set to automatically carry out actions due to the over-threshold vibrations); therefore, in most cases, this formula can be treated as being accurate (the maximum error, e.g., in the case of 30% SAGE, is about 10%) for the engineering calculation. However, for the cases of more than 30% SAGE, this formula should be improved. In this paper, we mainly focus on the effect of the SAGE forms on the rotor UMP; the refined analysis about the formula simplification error will not be taken due to the space limitation.

Then the MFD in the air-gap is

$$B(\alpha_m, t) = f(\alpha_m, t)\Lambda(\alpha_m) = F_1 \cos(\omega_r t - \alpha_m - \beta) \cdot \left[\Lambda_0 + \Lambda_s \cos\alpha_m + \sum \Lambda'_{sn} \cos(\alpha_m + \theta_n)\right]. \tag{4}$$

2.2. UMP Deduction. The air-gap MFD will be asymmetrical in different extents due to different SAGE forms, which will further generate rotor UMP and result in vibrations. In this paper, we employ (5), which is widely used by scholars [3], to obtain the unit magnetic force firstly and then deduce the UMP formulas via integral operation indicated in (6):

$$q(\alpha_m, t) = \frac{B^2(\alpha_m, t)}{2\mu_0} \tag{5}$$

$$F_x = \int_0^{2\pi} q(\alpha_m, t) \cos\alpha_m d\alpha_m$$
$$F_y = \int_0^{2\pi} q(\alpha_m, t) \sin\alpha_m d\alpha_m, \tag{6}$$

Table 1: UMP amplitudes and influential factors.

SAGE cases	Components		Amplitudes	Influential factors
Rotor offset	DC component	F_x	$2\Lambda_0\Lambda_s LRF_1^2\pi/4\mu_0$	Rotor offset degree, exciting current
		F_y	0	—
	$2f$ pulsating component	F_x	$\Lambda_0\Lambda_s LRF_1^2\pi/4\mu_0$	Rotor offset degree, exciting current
		F_y	$\Lambda_0\Lambda_s LRF_1^2\pi/4\mu_0$	
Stator deformation	DC component	F_x	$2\Lambda_0\Sigma\Lambda'_{sn}\cos\theta_n LRF_1^2\pi/4\mu_0$	Stator deformation numbers & degrees, Deformation locations and directions, and exciting current
		F_y	$2\Lambda_0\Sigma\Lambda'_{sn}\sin\theta_n LRF_1^2\pi/4\mu_0$	
	$2f$ pulsating component	F_x	$\Lambda_0\Sigma\Lambda'_{sn}\cos\theta_n LRF_1^2\pi/4\mu_0$	
		F_y	$\Lambda_0\Sigma\Lambda'_{sn}\cos\theta_n LRF_1^2\pi/4\mu_0$	
Mixed SAGE	DC component	F_x	$(2\Lambda_0\Lambda_s+2\Lambda_0\Sigma\Lambda'_{sn}\cos\theta_n) LRF_1^2\pi/4\mu_0$	Rotor offset degree, stator deformation numbers & degrees, deformation locations and directions, and exciting current
		F_y	$2\Lambda_0\Sigma\Lambda'_{sn}\sin\theta_n LRF_1^2\pi/4\mu_0$	
	$2f$ pulsating component	F_x	$(\Lambda_0\Lambda_s+\Lambda_0\Sigma\Lambda'_{sn}\cos\theta_n) LRF_1^2\pi/4\mu_0$	
		F_y	$(\Lambda_0\Lambda_s+\Lambda_0\Sigma\Lambda'_{sn}\cos\theta_n) LRF_1^2\pi/4\mu_0$	

where μ_0 is the air permeability and the final rotor UMPs in different SAGE cases are

$$F_x = 0$$
$$F_y = 0$$

Case 0: normal condition

$$F_x = \frac{LRF_1^2\pi}{4\mu_0}\left[2\Lambda_0\Lambda_s + \Lambda_0\Lambda_s\cos(2\omega t - 2\beta)\right]$$
$$F_y = \frac{LRF_1^2\pi}{4\mu_0}\left[\Lambda_0\Lambda_s\sin(2\omega t - 2\beta)\right]$$

Case I: rotor offset

$$F_x = \frac{LRF_1^2\pi}{4\mu_0}\left[2\Lambda_0\sum\Lambda'_{sn}\cos\theta_n + \Lambda_0\sum\Lambda'_{sn}\cos(2\omega t - 2\beta + \theta_n)\right]$$
$$F_y = \frac{LRF_1^2\pi}{4\mu_0}\left[2\Lambda_0\sum\Lambda'_{sn}\sin\theta_n + \Lambda_0\sum\Lambda'_{sn}\sin(2\omega t - 2\beta + \theta_n)\right]$$

Case II: stator deformation

$$F_x = \frac{LRF_1^2\pi}{4\mu_0}\left[2\Lambda_0\Lambda_s + 2\Lambda_0\sum\Lambda'_{sn}\cos\theta_n + \Lambda_0\Lambda_s\cos(2\omega t - 2\beta) + \Lambda_0\sum\Lambda'_{sn}\cos(2\omega t - 2\beta - \theta_n)\right]$$
$$F_y = \frac{LRF_1^2\pi}{4\mu_0}\left[2\Lambda_0\sum\Lambda'_{sn}\sin\theta_n + \Lambda_0\Lambda_s\sin(2\omega t - 2\beta) + \Lambda_0\sum\Lambda'_{sn}\sin(2\omega t - 2\beta - \theta_n)\right]$$

Case III: mixed condition. (7)

It is suggested from (7) that SAGE will induce a DC UMP component and pulsating UMP components at $2f$. Moreover, the component amplitudes will vary due to different SAGE cases. Qualitatively, the DC component will not bring in vibrations but generate a deformation tendency to the rotor after a long period action, while the pulsating force components will induce radial vibrations at the pulsating frequency, that is, $2f$. More details about the vibration characteristics will be studied in the next section.

2.3. Vibration Characteristics Analysis. As previously mentioned, radial rotor vibrations at $2f$ will be caused by SAGE. However, the vibration intensity for each case will be different. The UMP amplitudes with respect to different SAGE cases are indicated in Table 1.

As is shown in Table 1, no matter what kind of SAGE happens in the generator, the UMP amplitudes are always related to the SAGE degrees and the exciting current value. As SAGE increases, the factors Λ_s and Λ'_{sn} will be increased, resulting in the increment of the UMP amplitudes and the vibration intensity. As the exciting current rises, the factor F_1 (the composite MMF) will be increased, also resulting in the enlargement of the UMP amplitudes and the rotor vibration magnitudes. The final UMP will generally direct to the position where the air-gap is smaller.

In the case of rotor offset, the UMP formula is relatively simple, as indicated in (7). This kind of SAGE is most frequently studied by scholars and usually called rotor eccentricity in citations. It is commonly caused by the malposition or damage of the bearings and the misalignment of the couplers. The MFD on the smaller side of the air-gap will be more intensive, while on the other side it will be sparser. Therefore, the UMP direction will cross along from the larger air-gap side to the smaller air-gap side, as indicated in Figure 3(a).

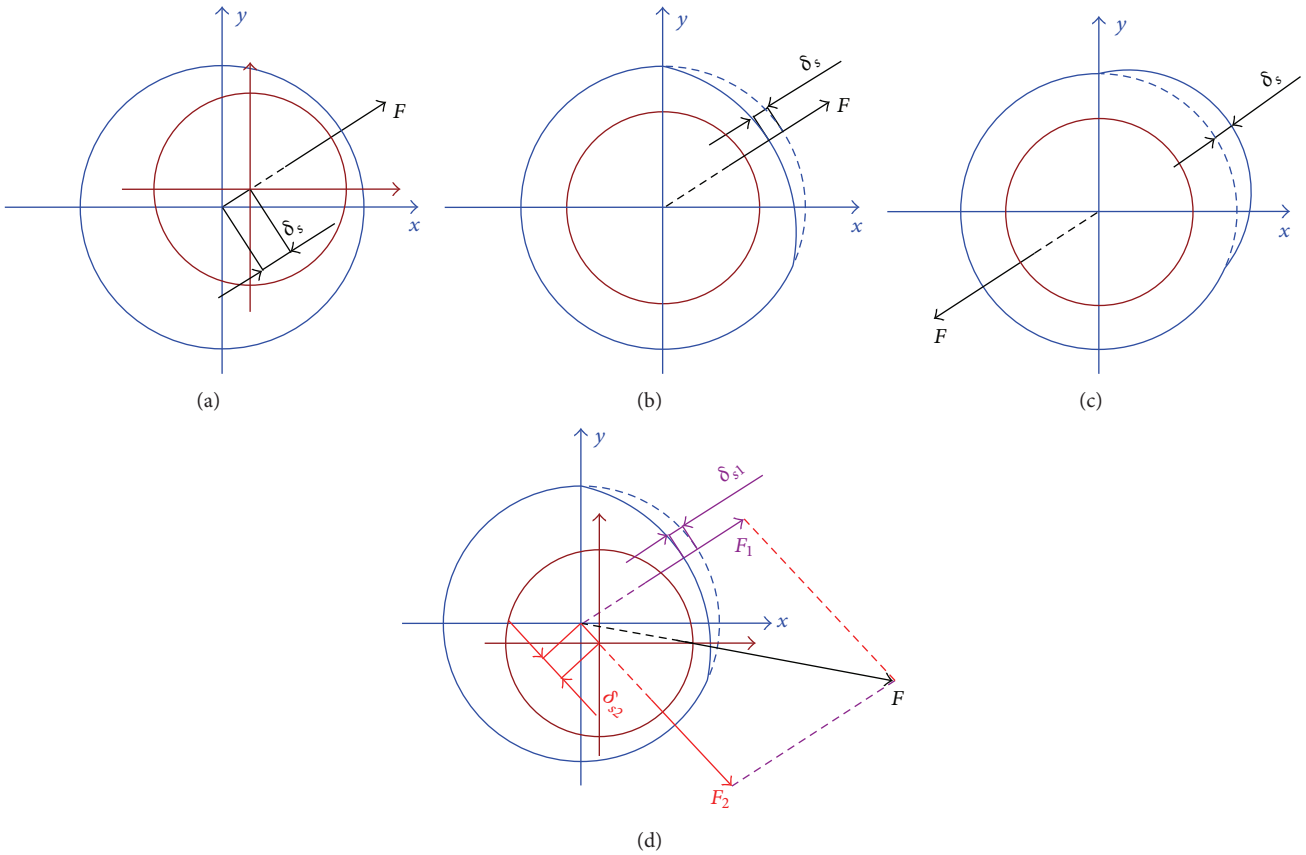

Figure 3: UMP directions for typical SAGE cases: (a) rotor offset, (b) stator concave deformation, (c) stator convex deformation, and (d) mixed SAGE composed of stator deformation and rotor offset.

Differently, in the case of stator deformation, it is possible that the UMP is zero. This will only occur when the deformations are symmetrically distributed in preciseness, as indicated in (7). In this case, there will be no vibration caused by this kind of SAGE. However, for most cases, the deformations are not critically asymmetrical, so that the induced UMP will bring in vibrations at $2f$. As indicated in (7) and Table 1, the UMP is related to the deformation number n, the level of deformation Λ'_{sn}, and the angle θ_n between the nth deformation and the X axis. Besides, the direction of the UMP is also associated with the eccentric direction. In theory, the larger the air-gap is, the greater the magnetoresistance will be. Therefore, the direction of the UMP will be directed from the larger side of the air-gap to the smaller side, as indicated in Figures 3(b) and 3(c). And as Λ'_{sn} increases, the UMP will be increased as well.

To be more specific, we take the case whose deformation number $n = 1$ for an example. This example case can be frequently induced due to the uneven heating and stressing. The rotor UMP formulas for the stator concave (δ'_{sn}) condition and the convex ($-\delta'_{sn}$) condition when $\theta_1 = 0^\circ$, respectively, reduce to

$$F_x = \frac{LRF_1^2\pi}{4\mu_0}\left[2\Lambda_0\Lambda'_{sn} + \Lambda_0\Lambda'_{sn}\cos\left(2\omega t - 2\beta\right)\right]$$
$$F_y = \frac{LRF_1^2\pi}{4\mu_0}\Lambda_0\Lambda'_{sn}\sin\left(2\omega t - 2\beta\right)$$
$$F_x = -\frac{LRF_1^2\pi}{4\mu_0}\left[2\Lambda_0\Lambda'_{sn} + \Lambda_0\Lambda'_{sn}\cos\left(2\omega t - 2\beta\right)\right]$$
$$F_y = -\frac{LRF_1^2\pi}{4\mu_0}\Lambda_0\Lambda'_{sn}\sin\left(2\omega t - 2\beta\right). \quad (8)$$

It can be seen that the UMP direction of the concave condition is opposite to the convex condition (also indicated in Figures 3(b) and 3(c)), while their amplitudes have the same formulas. However, since the concave case will reduce the average value of the air-gap length g_0 and then decrease the magnetic resistance, the general permeance Λ_0 in this case is larger than that of the convex case (see (3)). Consequently, the UMPs will be greater and vibrations will be more intensive.

The special SAGE case which is mixed with rotor offset and stator deformation at the same time can be treated as a superposition of these two single conditions. This can be confirmed by comparing the UMP formulas shown in (7). The final UMP direction needs to be calculated by means of parallelogram law, as indicated in Figure 3(d). And the final UMP direction is affected by the stator deformation numbers, deformation positions, and deformation degrees, as well as the rotor offset positions and offset degrees, in the meantime.

It is easy to comprehend that, to precisely describe the rotor vibration, both the intensity and the direction should

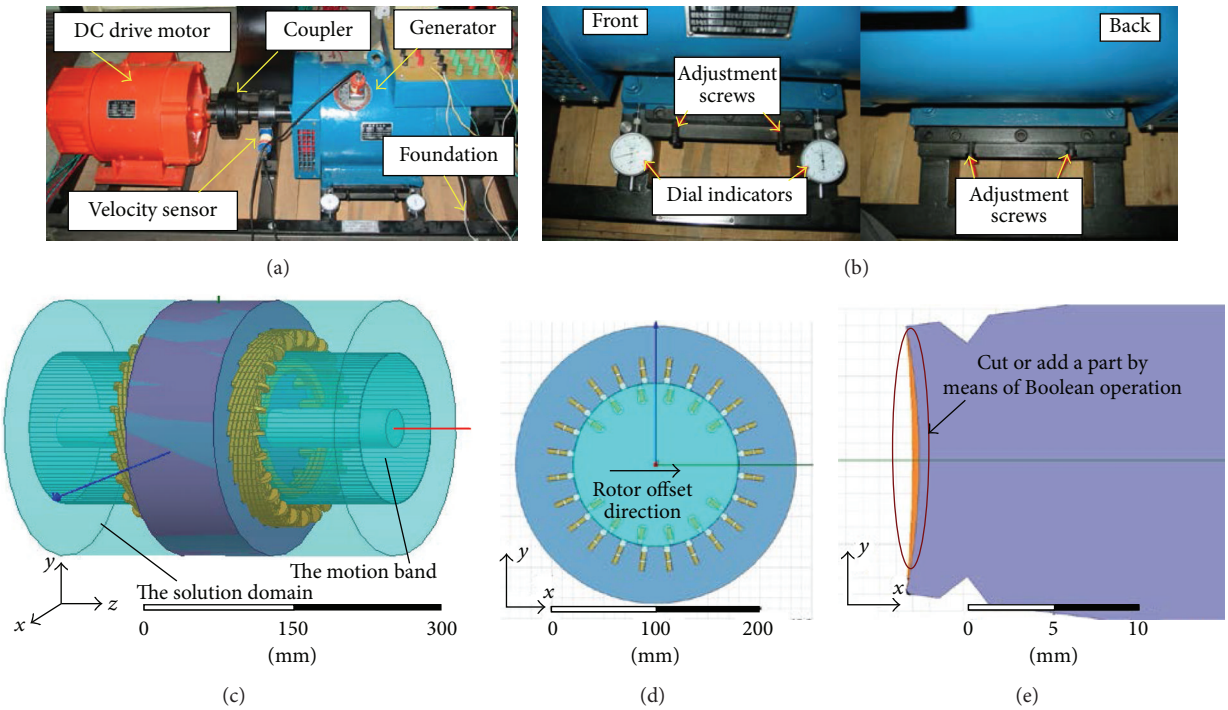

Figure 4: The study object: SDF-9 type fault simulating generator: (a) overall appearance, (b) method to set experimental rotor offset SAGE, (c) FEM model, (d) method to set simulating rotor offset, and (e) method to set simulating stator deformation.

be taken into consideration, of which the intensity depends on the factors indicated in Table 1, while the direction generally follows the UMP and is affected by the factors mentioned previously (see the above paragraph). For the sake of convenience, we describe the direction of the UMP and vibration by using the X-component and the Y-component, just like the formula decomposition using F_x and F_y (see (7)).

3. Experiment and Simulation Study

3.1. Method and Setting. Experiments are taken on a SDF-9 type nonsalient fault simulating generator in the National Key Lab of New Energy and Electric Power System, North China Electric Power University, as indicated in Figure 4(a). This generator is also modeled for the following simulation studies. The primary parameters of the generator are shown in Table 2.

The rotor of the generator is fixed to the foundation by the bearing block, while the stator can be horizontally moved by adjusting the four screws on the generator, and the movement performance can be precisely controlled by the two dial indicators, as illustrated in Figure 4(b). However, this generator can only simulate SAGE fault caused by rotor offset, while the other two SAGE cases (the stator deformation and the mixed condition composed of rotor offset and stator deformation) are not able to be simulated. Eclectically, we set up a FEM model of the generator to perform a numerical simulation, as indicated in Figure 4(c), and the methods to set rotor offset and stator deformation are shown in Figures 4(d) and 4(e), respectively. The mixed SAGE can be simulated by taking the rotor offset and the stator deformation operations at the same time.

Table 2: Primary parameters of SDF-9 type generator.

Parameters	Values
Rated capacity	7.5 kVA
Rated voltage	400 V
Power factor	$\cos\varphi = 0.8$
Rated rotating speed	$n_r = 3000$ rpm
Number of pole-pairs	$p = 1$
Radial air-gap length	$g_0 = 0.8$ mm
Axial air-gap length	$l = 100$ mm
Number of stator slots	$Z_1 = 24$
Ratio of pitch to polar distance	$k_y = y/\tau = 0.83$
Pitch-shortening value	$k_p = 0.966$
Distribution coefficient	$k_d = 0.958$
Number of parallel branches	$\alpha = 2$

During the experiment and the simulation, the exciting current is set to 0.4 A and the rotating speed is 3000 rpm (the fundamental frequency is 50 Hz). The rotor vibration is sampled by the velocity sensor (CD-21s type sensor made by Far East Vibration (Beijing) System Engineering Technology Co., Ltd., with the sensitivity 30 mv/mm/s) on the bearing block, with the sampling frequency 10 k Hz. The generator is firstly operated in normal condition to collect the reference UMP and vibration data. Then different SAGE conditions are applied to the generator to obtain the faulty signals. We carry out 0.1 mm ($\delta_s = 12.5\%$), 0.2 mm ($\delta_s = 25\%$), and 0.3 mm

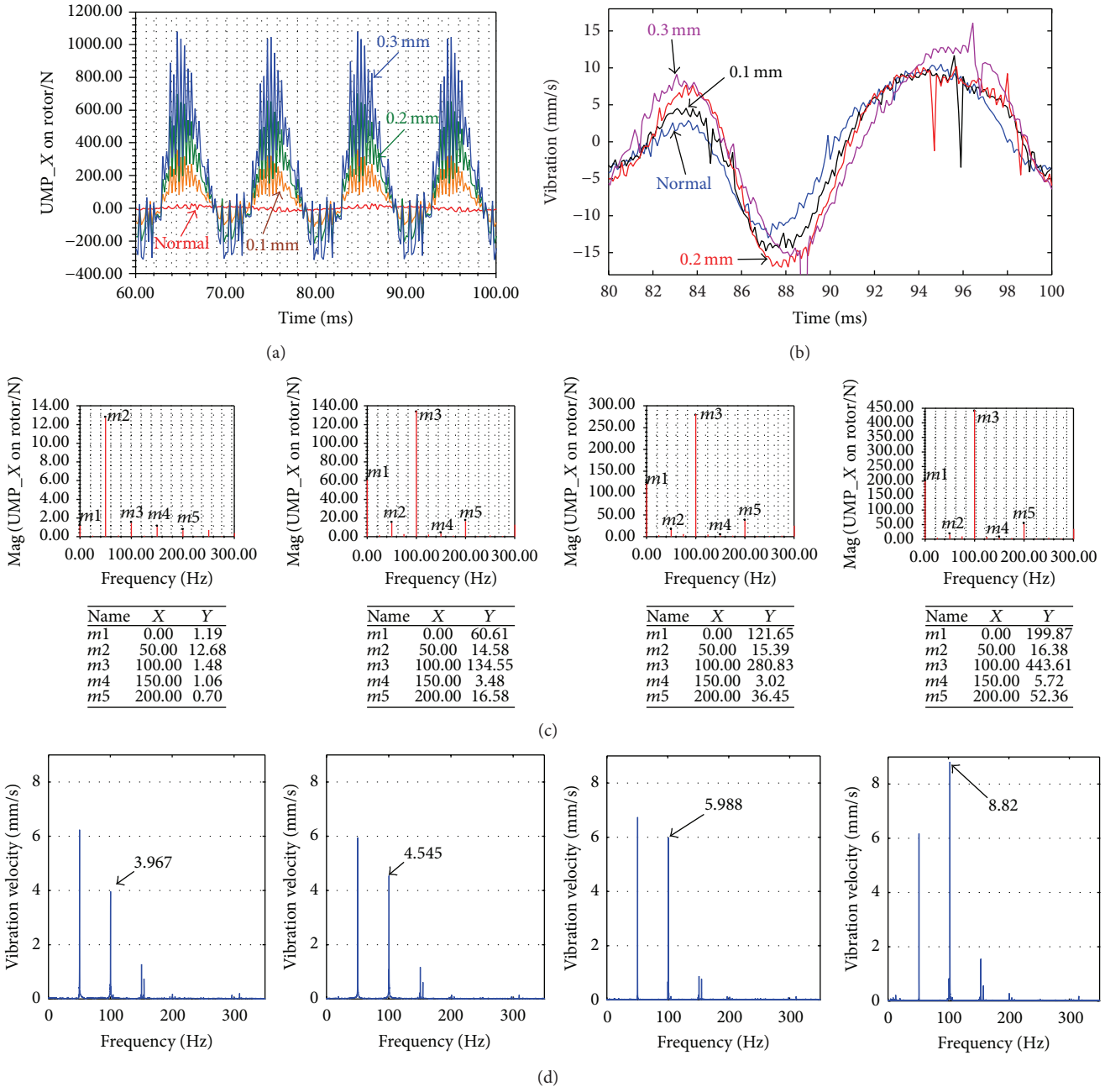

FIGURE 5: Rotor UMP and vibration results for rotor offset cases: (a) UMP curves by FEM calculation in x direction, (b) tested vibration curves in x direction, and ((c) and (d)) UMP spectra and vibration spectra, respectively, for normal condition, 0.1 mm rotor offset, 0.2 mm rotor offset, and 0.3 mm rotor offset (from left to right) in x direction.

(δ_s = 37.5%) rotor offset conditions for the experiment, while for the FEM simulations the SAGE cases are much more complete. Detailed settings for simulating conditions are shown in Table 3, where the stator deformation condition with the number $n = 4$ is actually a stator core ellipse case.

3.2. Results and Discussion

3.2.1. Impact of Rotor Offset. The calculated UMP by FEM simulation and the tested vibration by the experiment are shown in Figure 5. As indicated in (7), the UMPs in X direction and Y direction have the same expression forms except the DC components. Limited by the space, in this paper, we primarily study the UMP in X direction (the experimental vibration data is also picked up in this direction).

As shown in Figure 5, obviously, the tested vibration result well accords with the simulated data. As the rotor offset is increased, both the UMP and the radial vibration at 0 Hz (the DC component, reflecting the mean value of the curves) and 100 Hz (the 2nd harmonic component) will be prominently

Table 3: Setting conditions for FEM simulation.

Conditions	Rotor offset	Stator deformation			Mixed SAGE
Condition 1	$\delta_s = 12.5\%$	$n = 1$ $\theta_1 = 0^\circ$ $\delta s_1 = 12.5\%$	$n = 1$ $\theta_1 = 0^\circ$ $\delta s_1 = -12.5\%$	$n = 4$ $\theta_1 = 0^\circ, \theta_2 = 180^\circ, \theta_3 = 270^\circ, \theta_4 = 90^\circ$ $\delta s_1 = \delta s_2 = 12.5\%, \delta s_3 = \delta s_4 = -12.5\%$	$n = 4$ $\theta_1 = 0^\circ, \theta_2 = 180^\circ, \theta_3 = 270^\circ, \theta_4 = 90^\circ$ $\delta s_1 = \delta s_2 = 12.5\%, \delta s_3 = \delta s_4 = -12.5\%$ $\delta_s = 12.5\%$
Condition 2	$\delta_s = 25\%$	$n = 1$ $\theta_1 = 0^\circ$ $\delta s_1 = 25\%$	$n = 1$ $\theta_1 = 0^\circ$ $\delta s_1 = -25\%$	$n = 4$ $\theta_1 = 0^\circ, \theta_2 = 180^\circ, \theta_3 = 270^\circ, \theta_4 = 90^\circ$ $\delta s_1 = \delta s_2 = 25\%, \delta s_3 = \delta s_4 = -25\%$	$n = 4$ $\theta_1 = 0^\circ, \theta_2 = 180^\circ, \theta_3 = 270^\circ, \theta_4 = 90^\circ$ $\delta s_1 = \delta s_2 = 25\%, \delta s_3 = \delta s_4 = -25\%$ $\delta_s = 25\%$
Condition 3	$\delta_s = 37.5\%$	$n = 1$ $\theta_1 = 0^\circ$ $\delta s_1 = 37.5\%$	$n = 1$ $\theta_1 = 0^\circ$ $\delta s_1 = -37.5\%$	$n = 4$ $\theta_1 = 0^\circ, \theta_2 = 180^\circ, \theta_3 = 270^\circ, \theta_4 = 90^\circ$ $\delta s_1 = \delta s_2 = 37.5\%, \delta s_3 = \delta s_4 = -37.5\%$	$n = 4$ $\theta_1 = 0^\circ, \theta_2 = 180^\circ, \theta_3 = 270^\circ, \theta_4 = 90^\circ$ $\delta s_1 = \delta s_2 = 37.5\%, \delta s_3 = \delta s_4 = -37.5\%$ $\delta_s = 37.5\%$

magnified; see Figures 5(c) and 5(d). This well follows the theoretical analysis presented previously. However, it is also suggested from Figure 5(c) that, besides the DC component and the 2nd harmonic component, the 4th harmonic component (200 Hz) of the UMP also has a considerable increment. This has not been indicated in (7) due to the ignoring of the higher order components of the MMF. Actually, the MFD and the MMF should have each odd harmonic component [29]; therefore the square operation in (5) will generate each even harmonic component, with the amplitude in inverse proportion to the harmonic order. This means, not only the 2nd and the 4th harmonic components, but also all of the even harmonic components will be increased. The higher the even harmonic order is, the less the amplitude will be increased.

Theoretically, the rotor should have no vibrations in normal condition due to the tiny UMP value very close to zero, as indicated in (7) and Figure 5(a). However, the result indicated in Figure 5(d) shows that there are vibrations of each harmonic existing. This is mainly caused by the internal asymmetry such as the unsymmetrical distribution of the windings inside the generator and the external nonfault environmental factors. To remove the influence of this mismatch between the theoretical analysis and the experimental phenomena, these vibration amplitudes of each harmonic component in normal condition are treated as a null shift of the experiment system, and the SAGE vibration amplitudes are subtracted by these normal ones so that the actual vibrations caused by the fault can be obtained. Quantitatively, the vibration velocity at $2f$ increases 14.6%, 50.9%, and 122.3% from normal condition to 0.1 mm (12.5%), 0.2 mm (25%), and 0.3 mm (37.5%) rotor offset, respectively, while other harmonic components have little changes. This is consistent with the theory analysis and the simulation results.

3.2.2. Impact of Stator Deformation. In the case of $n = 1$ and $\theta_1 = 0^\circ$, the time domain curves of the UMP for the stator concave condition and the convex condition are shown in Figures 6(a) and 6(b), respectively, while the spectra are indicated in Figures 6(c) and 6(d). It is shown that the UMP under the concave condition is larger than that under the convex condition. This is because the concave condition actually reduces the average air-gap length, while the convex condition increases the average air-gap length. The MFD is in inverse proportion to the air-gap eccentricity. The smaller the air-gap is, the larger the MFD will be. As indicated in (5) and (6), the UMP actually follows the developing tendency of the MFD. Therefore, the stator concave condition, which equivalently reduces the air-gap length, makes the UMP larger than that of convex condition.

In addition, as the deformation increases, the 2nd and 4th harmonic components of the UMP will be increased. For the concave condition, the UMP has a larger value at the positive peak than the negative peak. Moreover, the surrounding area by the UMP curve above the zero line is more than that below the zero line. This indicates that the UMP generally acts along the positive direction (x direction), to which is also the minimum air-gap length location. However, for the convex condition, the situation will be opposite. This is in accordance with the previous theoretical analysis.

In addition to the stator concave and convex deformation, there is still another form of stator deformation, that is, the overall elliptical deformation which widely exists in generators with different extents. Figure 7 represents the rotor UMP under different ellipse deformation conditions in the case that $n = 4$, $\delta'_{s1} = \delta'_{s2}$, $\delta'_{s3} = \delta'_{s4}$, $\theta_1 = 0^\circ$, $\theta_2 = 180^\circ$, $\theta_3 = 270^\circ$, and $\theta_4 = 90^\circ$. Theoretically, according to (4), since the decrease of the air-gap caused by δ_{s3} and δ_{s4} is generally equivalent to the increment caused by $-\delta_{s3}$ and $-\delta_{s4}$ (see Figure 2(e)) due to the volume invariance of the stator core, the UMP should be very close to zero, which means in this case that the rotor UMP is almost unchanged. As indicated in Figure 7, it is shown that the rotor UMP under the stator ellipse deformation condition is very similar to that in normal condition. This is in accordance with the theoretical result.

3.2.3. Impact of Mixed SAGE. The more common case is that the rotor offset exists together with the stator deformation, that is, the mixed SAGE. Practically, the concave deformation and the convex deformation conditions appear much less than the ellipse deformation condition. Therefore, we focus on the mixed SAGE composed of rotor offset and stator ellipse deformation. Figure 8 represents the rotor UMP

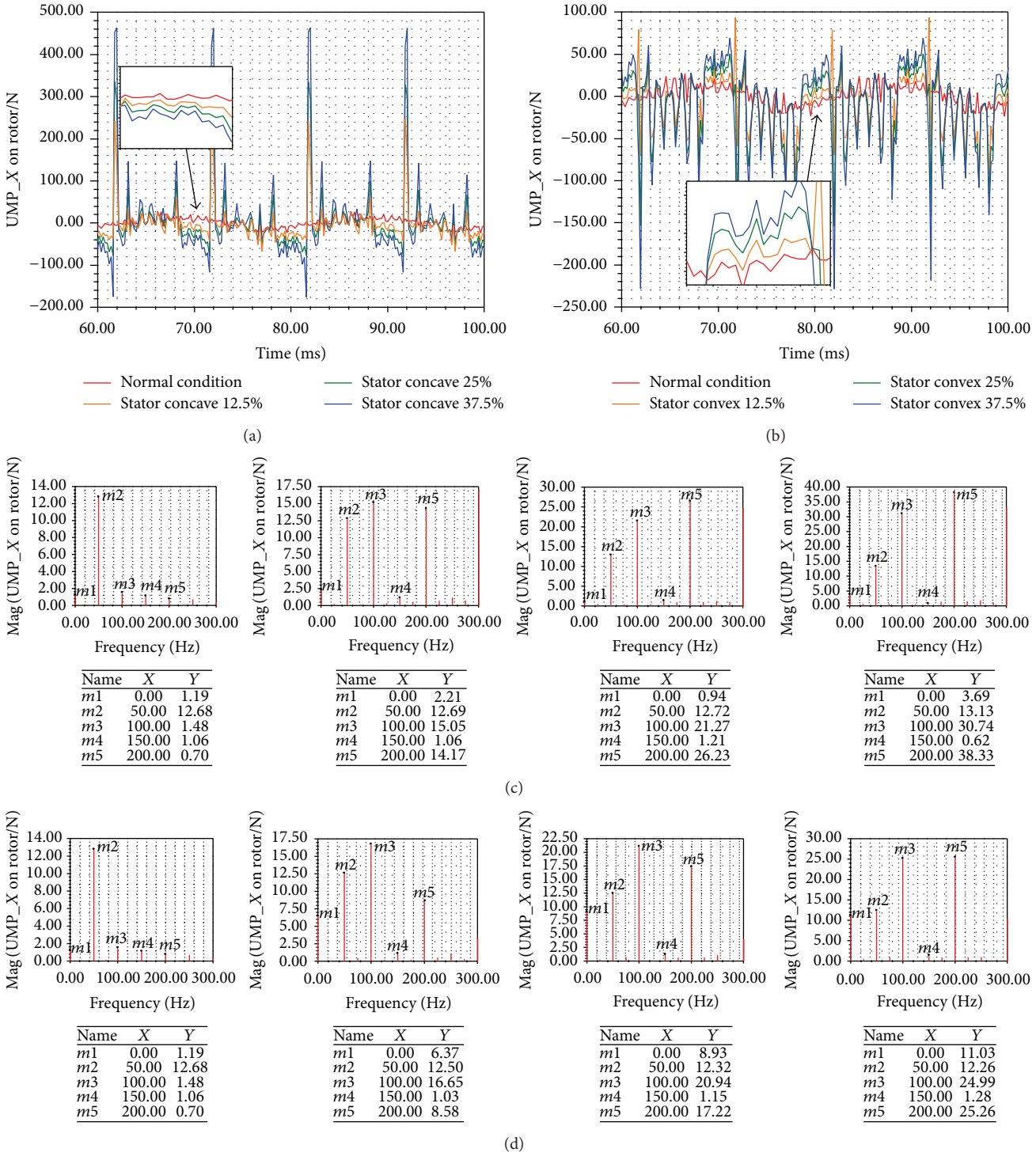

FIGURE 6: Rotor UMP caused by stator deformation: (a) UMP curves in concave condition, with $n = 1$, $\delta'_{s1} = \delta'_{sn}$, and $\theta_1 = 0^\circ$, (b) UMP curves in convex condition, with $n = 1$, $\delta'_{s1} = -\delta'_{sn}$, and $\theta_1 = 0^\circ$, and ((c) and (d)) UMP spectra in concave case and convex case with respect to normal condition, 12.5% deformation, 25% deformation, and 37.5% deformation, respectively (from left to right).

results under different mixed SAGE conditions. As can be seen from the figure, the rotor UMP is about zero in normal condition, while it begins to increase when the mixed SAGE occurs. The 2nd harmonic component has a most obvious amplitude increment. Also, the increment of the 4th harmonic component is more evident than the other harmonic components. The reason for this has been explained in Section 3.2.1.

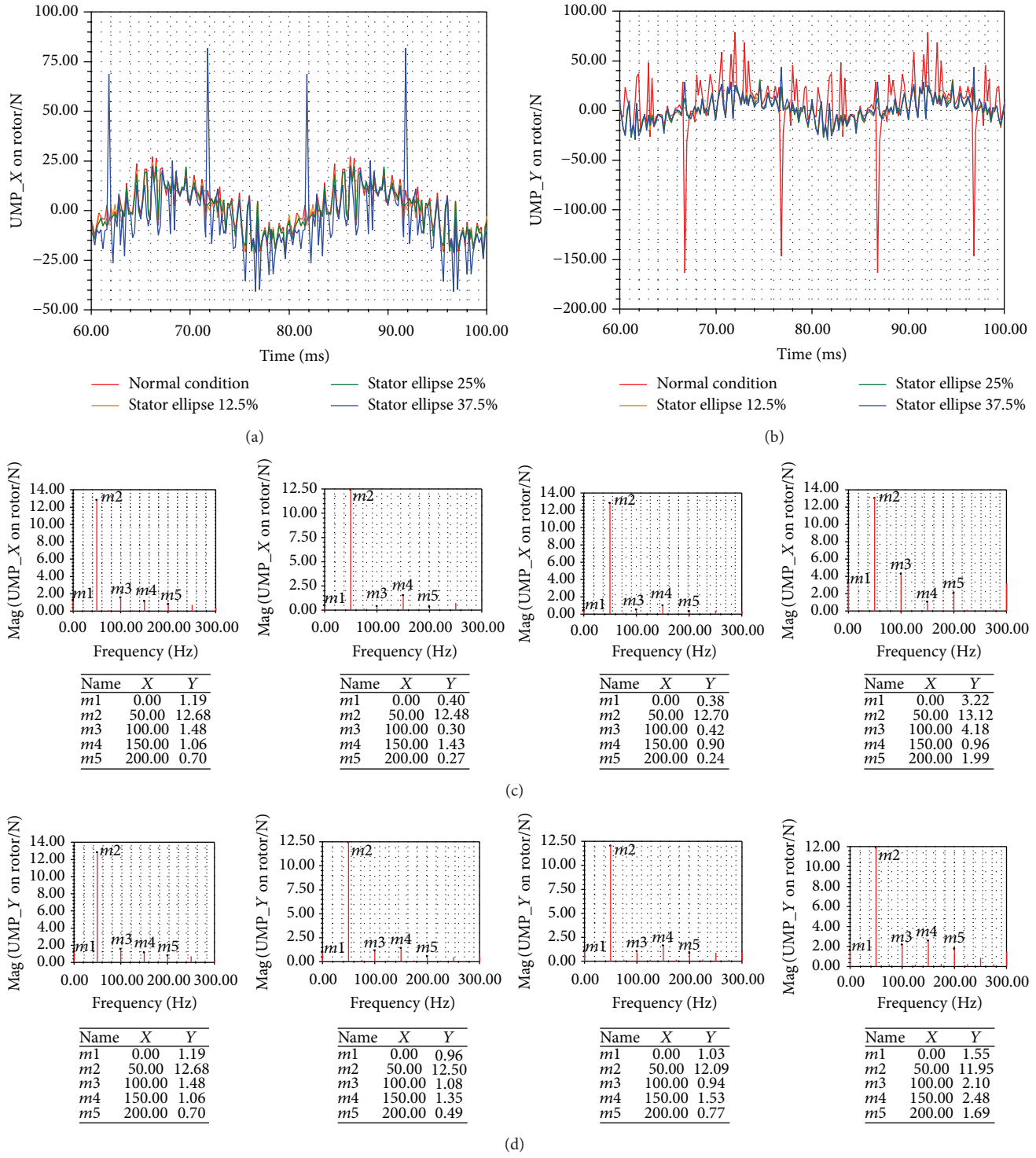

Figure 7: Rotor UMP caused by overall elliptical deformation of stator core: ((a) and (b)) time domain waves in X and Y direction, respectively, and ((c) and (d)) UMP spectra in X and Y direction, respectively, under normal condition, 12.5% stator core ellipse, 25% stator core ellipse, and 37.5 stator core ellipse (from left to right).

Generally speaking, the UMP developing tendency and the key UMP characteristics are similar to the other two SAGE conditions. So there is a key problem, that is, how to identify the feature differences of the UMP caused by different kinds of SAGE. The statistics data of the 2nd harmonic component of the rotor UMP, which is the key characteristic component caused by different SAGE forms, is indicated in Table 4.

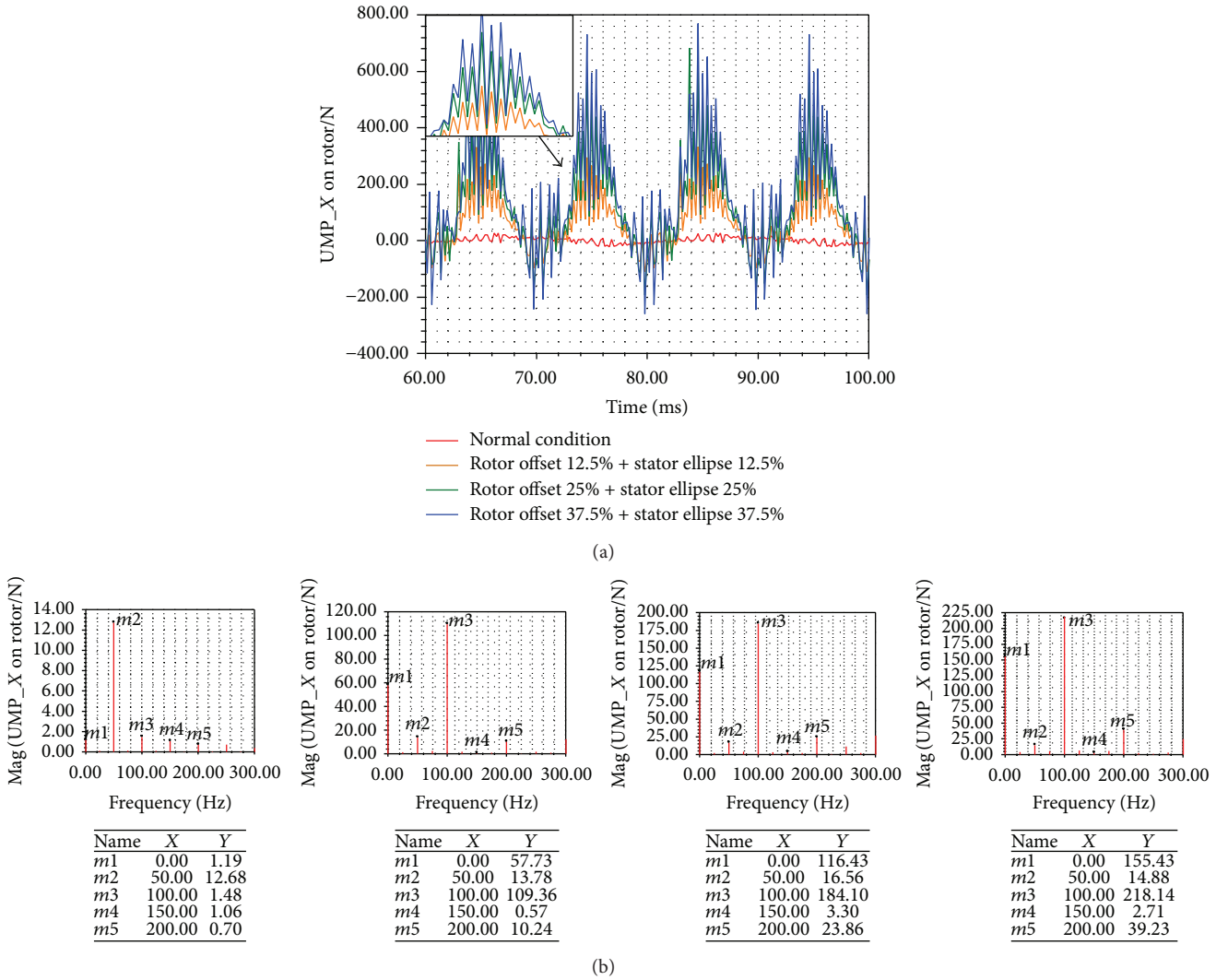

Figure 8: Rotor UMP caused by mixed eccentricity faults: (a) time domain waves and (b) UMP spectra, respectively, in the case of 12.5% rotor offset and 12.5% stator core ellipse, 25% rotor offset and 25% stator core ellipse, and 37.5% rotor offset and 37.5% stator core ellipse (from left to right).

Table 4: UMP amplitudes of different SAGE cases.

SAGE cases		$2f$ pulsating component amplitudes under different SAGE degree			
		Normal	δ = 12.5%	δ = 25%	δ = 37.5%
Rotor offset		1.48	134.55	280.83	443.61
Stator deformation	Concave		15.05	21.27	30.74
	Convex		16.65	20.94	24.99
	Ellipse		0.30	0.42	4.18
Mixed SAGE composed of rotor offset and ellipse			109.36	184.10	218.14

As indicated in Table 4, it is shown that the rotor offset condition will produce a largest UMP value at $2f$, while the ellipse condition will induce the smallest UMP. In addition, the impact of the stator concave and convex condition on the UMP is also much smaller than the rotor offset condition, while the mixed SAGE case will generate the second largest UMP.

In fact, qualitatively, the mixed SAGE composed of rotor offset and stator convex and concave deformation (especially the concave deformation) will actually bring in larger UMP

than the mixed one indicated in the table. In other words, the rotor offset has a most sensitive effect on the rotor UMP, and then the second, the third, and the fourth sensitive forms are the mixed SAGE conditions, respectively, composed of the rotor offset and the stator concave deformation, the rotor offset and the stator convex deformation, and the rotor offset and the stator ellipse deformation. The fifth and the sixth sensitive conditions are the single stator concave and convex deformation, respectively, while the single stator ellipse condition has the weakest impact on the rotor UMP.

4. Conclusion

This paper investigates the impact of different SAGE forms on the rotor UMP. The whole work is primarily carried out through the theoretical analysis and the numerical FEM calculation, together with some experiment studies. Main conclusions drawn from the work are as follows.

(1) The occurrence of SAGE, no matter which kind it is, will bring in amplitude increments at each even harmonic component of the UMP and the rotor vibration, especially the 2nd harmonic component. The severer the SAGE is, the more the amplitude increment will be caused.

(2) Among the single SAGE types, the rotor offset has the most sensitive effect on the rotor UMP and vibration, while the stator ellipse deformation has the weakest impact. The stator concave and convex deformation forms have the second and the third sensitive impact.

(3) The mixed SAGE conditions composed of rotor offset and stator concave, stator convex, and stator ellipse deformation will induce a larger rotor UMP and drastic vibration compared to the single concave, convex, and ellipse deformation, but meanwhile a smaller rotor UMP and weaker vibration than the single rotor offset form.

These conclusions can be potentially used to improve the identification accuracy of SAGE fault. Practically, in most cases, the identification work can only conclude whether the generator has a SAGE fault but cannot exactly identify the detailed forms of SAGE. However, different SAGE forms will lead to various performances. For example, the stator ellipse deformation without a serious extent can be generally ignored due to the very tiny UMP induced by this kind of SAGE, while the rotor offset form needs careful modification work on the rotor to avoid further deterioration and potential damage. Based on the work proposed in this paper, a more advanced application method may be developed, which will be beneficial for the SAGE fault monitoring and control.

Competing Interests

The authors declare that they have no competing interests.

Acknowledgments

This work is supported by the National Natural Science Foundation of China (no. 51307058), the Natural Science Foundation of Hebei Province, China (E2014502052, E2015502013), and the Chinese Fundamental Research Funds for the Central Universities (2015ZD27).

References

[1] L. T. Rosenberg, "Eccentricity, vibration, and shaft currents in turbine generators," *Transactions of the American Institute of Electrical Engineers. Part III: Power Apparatus and Systems*, vol. 74, no. 3, pp. 38–41, 1955.

[2] S. T. Wan and Y. L. He, "Analysis on stator circulating current characteristics of turbo-generator under eccentric faults," in *Proceedings of the IEEE 6th International Power Electronics and Motion Control Conference (IPEMC '09)*, pp. 2062–2067, IEEE, Wuhan, China, May 2009.

[3] S. T. Wan and Y. L. He, "Investigation on stator and rotor vibration characteristics of turbo-generator under air gap eccentricity fault," *Transactions of the Canadian Society for Mechanical Engineering*, vol. 35, no. 2, pp. 161–176, 2011.

[4] B. M. Ebrahimi, J. Faiz, and M. J. Roshtkhari, "Static-, dynamic-, and mixed-eccentricity fault diagnoses in permanent-magnet synchronous motors," *IEEE Transactions on Industrial Electronics*, vol. 56, no. 11, pp. 4727–4739, 2009.

[5] C. Bruzzese, "Diagnosis of eccentric rotor in synchronous machines by analysis of split-phase currents—part I: theoretical analysis," *IEEE Transactions on Industrial Electronics*, vol. 61, no. 8, pp. 4193–4205, 2014.

[6] C. Bruzzese, "Diagnosis of eccentric rotor in synchronous machines by analysis of split-phase currents—part II: experimental analysis," *IEEE Transactions on Industrial Electronics*, vol. 61, no. 8, pp. 4206–4216, 2014.

[7] J.-H. Zhu, A.-R. Qiu, and T. Guo, "Branch voltage of a salient pole synchronous generator with eccentric rotor and skewed slots," *Journal of Tsinghua University (Science and Technology)*, vol. 48, no. 4, pp. 453–456, 2008.

[8] C. Bruzzese and G. Joksimovic, "Harmonic signatures of static eccentricities in the stator voltages and in the rotor current of no-load salient-pole synchronous generators," *IEEE Transactions on Industrial Electronics*, vol. 58, no. 5, pp. 1606–1624, 2011.

[9] W. Doorsamy, A. A.-E. Abdallh, W. A. Cronje, and L. Dupré, "An experimental design for static eccentricity detection in synchronous machines using a Cramér-Rao lower bound technique," *IEEE Transactions on Energy Conversion*, vol. 30, no. 1, pp. 254–261, 2015.

[10] B. A. T. Iamamura, Y. Le Menach, A. Tounzi, N. Sadowski, and E. Guillot, "Study of static and dynamic eccentricities of a synchronous generator using 3-D FEM," *IEEE Transactions on Magnetics*, vol. 46, no. 8, pp. 3516–3519, 2010.

[11] M. Babaei, J. Faiz, B. M. Ebrahimi, S. Amini, and J. Nazarzadeh, "A detailed analytical model of a salient-pole synchronous generator under dynamic eccentricity fault," *IEEE Transactions on Magnetics*, vol. 47, no. 4, pp. 764–771, 2011.

[12] D. G. Dorrell, "Experimental behaviour of unbalanced magnetic pull in 3-phase induction motors with eccentric rotors and the relationship with tooth saturation," *IEEE Transactions on Energy Conversion*, vol. 14, no. 3, pp. 304–309, 1999.

[13] W.-L. Li, T. Li, X.-C. Zhang, and J.-M. Geng, "Calculation and analysis of high-speed permanent magnetic generator unilateral

magnetic force," in *Proceedings of the 11th International Conference on Electrical Machines and Systems (ICEMS '08)*, pp. 3284–3288, Wuhan, China, October 2008.

[14] L. Wang, R. W. Cheung, Z. Y. Ma, J. M. Ruan, and Y. Peng, "Finite-element analysis of unbalanced magnetic pull in a large hydro-generator under practical operations," *IEEE Transactions on Magnetics*, vol. 44, no. 6, pp. 1558–1561, 2008.

[15] G. M. Joksimovi, "Dynamic simulation of cage induction machine with air gap eccentricity," *IEE Proceedings—Electric Power Applications*, vol. 152, no. 4, pp. 803–811, 2005.

[16] I. Tabatabaei, J. Faiz, H. Lesani, and M. T. Nabavi-Razavi, "Modeling and simulation of a salient-pole synchronous generator with dynamic eccentricity using modified winding function theory," *IEEE Transactions on Magnetics*, vol. 40, no. 3, pp. 1550–1555, 2004.

[17] J. Faiz and M. Ojaghi, "Unified winding function approach for dynamic simulation of different kinds of eccentricity faults in cage induction machines," *IET Electric Power Applications*, vol. 3, no. 5, pp. 461–470, 2009.

[18] D. G. Dorrell and A. Salah, "Detection of rotor eccentricity in wound rotor induction machines using pole-specific search coils," *IEEE Transactions on Magnetics*, vol. 51, no. 11, pp. 1–4, 2015.

[19] Y. Calleecharan and J.-O. Aidanpää, "Stability analysis of an hydropower generator subjected to unbalanced magnetic pull," *IET Science, Measurement & Technology*, vol. 5, no. 6, pp. 231–243, 2011.

[20] D. G. Dorrell, M.-F. Hsieh, and Y. Guo, "Unbalanced magnet pull in large brushless rare-earth permanent magnet motors with rotor eccentricity," *IEEE Transactions on Magnetics*, vol. 45, no. 10, pp. 4586–4589, 2009.

[21] X. P. Xu, Q. K. Han, and F. L. Chu, "A four degrees-of-freedom model for a misaligned electrical rotor," *Journal of Sound and Vibration*, vol. 358, pp. 356–374, 2015.

[22] P. Pennacchi and L. Frosini, "Dynamical behaviour of a three-phase generator due to unbalanced magnetic pull," *IEE Proceedings—Electric Power Applications*, vol. 152, no. 6, pp. 1389–1400, 2005.

[23] H. Mahmoud and N. Bianchi, "Eccentricity in synchronous reluctance motors—part I: analytical and finite-element models," *IEEE Transactions on Energy Conversion*, vol. 30, no. 2, pp. 745–753, 2015.

[24] S. M. Mirimani, A. Vahedi, F. Marignetti, and E. De Santis, "Static eccentricity fault detection in single-stator-single-rotor axial-flux permanent-magnet machines," *IEEE Transactions on Industry Applications*, vol. 48, no. 6, pp. 1838–1845, 2012.

[25] G.-J. Tang, Y.-L. He, S.-T. Wan, and L. Xiang, "Investigation on stator vibration characteristics under air-gap eccentricity and rotor short circuit composite faults," *Journal of the Brazilian Society of Mechanical Sciences and Engineering*, vol. 36, no. 3, pp. 511–522, 2014.

[26] K. Sawatani, K. Sano, and S. Ootake, "Stator frame deformation problem in large diameter hydro-generators," *IEEE Transactions on Energy Conversion*, vol. 1, no. 1, pp. 33–38, 1986.

[27] M. Valavi, A. Nysveen, R. Nilssen, and T. Rølvåg, "Slot harmonic effect on magnetic forces and vibration in low-speed permanent-magnet machine with concentrated windings," *IEEE Transactions on Industry Applications*, vol. 50, no. 5, pp. 3304–3313, 2014.

[28] C. Azuaje and A. Millan, "Stator deformation of large hydrogenerators and its effects on the machines," in *Proceedings of the IEEE PES Transmission & Distribution Conference and Exposition: Latin America (TDC '06)*, pp. 1–5, Caracas, Venezuela, August 2006.

[29] S. T. Wan, Y. L. He, G. J. Tang, and Y. G. Li, "Investigation on stator circulating current characteristics of turbogenerators under air gap eccentricity and rotor short-circuit composite faults," *Electric Power Components and Systems*, vol. 38, no. 8, pp. 900–917, 2010.